First Series of Transition-Metal-Layered Oxycarbonates: $Sr_4Fe_{2-x}M_xO_6CO_3$ (M = Sc, Ni, Co)

Y. Bréard, C. Michel,* A. Maignan, F. Studer, and B. Raveau

Laboratoire CRISMAT, UMR CNRS 6508, 6 Boulevard du Maréchal Juin, F14150 Caen Cedex, France

Received September 30, 2002. Revised Manuscript Received December 18, 2002

The possibility of synthesizing layered oxycarbonates, with nominal composition $Sr_4Fe_{2-x}M_xO_6CO_3$ (with M = Sc, Co, or Ni) involving trivalent scandium, cobalt, or nickel, with $0 \le x \le 2$ (M = Sc), $0 \le x \le 1.5$ (M = Co), and $0 \le x \le 1.1$ (M = Ni), is reported for the first time. The structural studies of $Sr_4Sc_2O_6CO_3$ and $Sr_4FeMO_6CO_3$ (M = Co and Ni) show that these three phases are closely related to the $n = 3$ member of the Ruddlesden−Popper family. They derive from the latter by replacing the middle layer of transition-metal octahedra by triangular CO_3 groups, with two different "flag" and "coat hanger" configurations. Magnetic behaviors that are fundamentally different from the magnetic behavior of $Sr_4Fe_2O_6CO_3$ are also reported.

Introduction

Transition-metal-layered oxycarbonates were first synthesized in the case of copper, with the compound $SrCuO_2CO_3$,[1] which consists of single perovskite layers stacked up with layers of triangular carbonate groups. Then several series of layered copper oxycarbonates derived from the $Sr_2CuO_2CO_3$ structure and from the 1201- or 2201-type structures by intergrowth and shearing mechanisms were generated and studied for their superconducting properties at high temperature (for a review see refs 2 and 3). The recent discovery of the iron-based layered oxycarbonate $Sr_4Fe_2O_6CO_3$[4,5] has shown that copper is not the only transition element that can form such layered compounds. The structure of $Sr_4Fe_2O_6CO_3$ can be considered as derived from the $n = 3$ member of the Ruddlesden and Popper (RP) series, $Sr_4Fe_3O_{10}$, by replacing, in the triple perovskite layer, the central slab of corner-sharing FeO_6 octahedra by triangular CO_3 groups. According to their mode of connection with the octahedra, the CO_3 groups exhibit two sorts of configurations labeled "flag" (Figure 1a) and "coat hanger" (Figure 1b), respectively. The first configuration is the only one adopted by copper oxycarbonates whereas $Sr_4Fe_2O_6CO_3$ exhibits a mixed "flag−coat hanger" configuration. In contrast to copper, $Sr_4Fe_2O_6CO_3$ is an insulator with Fe^{3+} cations magnetically ordered below 360 K. Recently, it has been shown that iron can be partially replaced by trivalent cations such as chromium[6] and manganese[7] up to at least 50%, leading to considerable changes in structural and magnetic properties. To understand the crystal chemistry and physics of this structural type, we have investigated the substitution of the other trivalent elements of the first transition series for iron. In this paper we demonstrate that the possibility of forming layered oxycarbonates $Sr_4Fe_{2-x}M_xO_6CO_3$ can be extended to nickel and cobalt with substitution rates larger than 50%, and to scandium with a substitution rate up to 100%. We show that the structure of all these oxycarbonates, like that of $Sr_4Fe_2O_6CO_3$, is characterized by a mixed flag−coat hanger configuration. All three compounds are insulators, and a particular spin glass behavior is observed for the nickel phase, whereas the cobalt compound exhibits a quasi-temperature-independent susceptibility value.

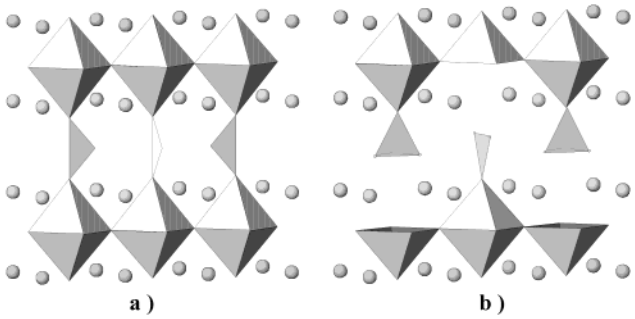

Figure 1. Flag (a) and coat hanger (b) configurations of the carbonate groups.

Experimental Section

Synthesis. The different samples with composition $Sr_4Fe_{2-x}M_xO_6CO_3$ were synthesized by direct solid-state reaction between adequate mixtures of precursors of which their nature depended on M: SrO, $SrCO_3$ Fe_2O_3, and Sc_2O_3 for M = Sc, SrO, SrO_2, $SrCO_3$, Fe_2O_3, and Co_3O_4 or NiO for M = Co or

* To whom correspondence should be addressed.

(1) Babu, T. G. N.; Fish, D. J.; Greaves, C. *J. Mater. Chem.* **1991**, *1*, 677.
(2) Goutenoire, F.; Hervieu, M.; Maignan, A.; Michel, C.; Martin, C.; Raveau, B. *Physica C* **1993**, *210*, 359.
(3) Maignan, A.; Pelloquin, D.; Malo, S.; Michel, C.; Hervieu, M.; Raveau, B. *Physica C* **1995**, *249*, 220.
(4) Yamaura, K.; Huang, O.; Lynn, J. W.; Erwin, R. W.; Cava, R. J. *J. Solid State Chem.* **2000**, *152*, 374.
(5) Bréard, Y.; Michel, C.; Hervieu, M.; Raveau, B. *J. Mater. Chem.* **2000**, *10*, 1043.
(6) Bréard, Y.; Michel, C.; Hervieu, M.; Raveau, B.; NGuyen, N.; Ducouret, A.; Studer, F.; Suard, E. *Chem. Mater.* **2001**, *13*, 2423.
(7) Bréard, Y.; Michel, C.; Hervieu, M.; Nguyen, N.; Studer, F.; Maignan, A.; Raveau, B.; Bourée, F. *J. Solid State Chem.*, in press.

10.1021/cm020468w CCC: $25.00
Published on Web 02/27/2003

Ni. In the two latter cases, the amount of SrO_2 was adjusted to keep an oxygen stoichiometry equal to 6. SrO was homemade by heating SrO_2 up to 1100 °C for 24 h and was introduced while still burning into a glovebox under an inert atmosphere to avoid carbonation or moisture. To try to improve the reactivity of nickel oxide, NiO was freshly prepared by decomposition at low temperature of nickel nitrate, in air. Last, SrO was weighed and well-mixed with the mixture of other precursors. The thoroughly ground powders were then pressed into the form of bars and introduced into silica tubes. This entire process was carried out in a drybox. The tubes were then sealed under vacuum and heated to 1200 °C for 12 h for scandium and up to 1100 °C for 12 h for nickel and cobalt. Heating and cooling to room temperature were performed in 6 h.

Structural Analysis. The electron diffraction (ED) investigation was carried out with a JEOL 200CX microscope, tilting around the crystallographic axes. The high-resolution electron microscopy (HREM) study was performed with a TOPCON 002B, operating at 200 kV and having a point resolution of 1.8 Å. Both microscopes are equipped with an EDS analyzer.

Phase purity was checked by X-ray diffraction using a Philips vertical diffractometer PW1830 equipped with a graphite secondary monochromator and working with Cu Kα radiation. Data were collected by step scanning of 0.025° (2θ) over an angular range of $5° < 2\theta < 120°$. X-ray diffraction patterns were used for lattice constant measurements.

Neutron powder diffraction data were collected at room temperature at LLB (Saclay, France) on the high-resolution 3T2 diffractometer, using the wavelength 1.2252 Å, in the angular range $6° < 2\theta < 126°$ with steps of 0.05° (2θ). The scattering lengths of the different atoms were those included in the Rietveld profile analysis program package (FULLPROF[8]).

The X-ray absorption spectra at Co, Ni, and Fe K-edges were recorded at room temperature in a classical transmission mode at the EXAFS I station (channel cut the monochromator) using the synchrotron radiation of the DCI storage ring of LURE (Orsay) working at 1.85 GeV with a 250-mA current. The energy resolution at the Co and Ni K-edge is estimated at 1.3 eV whereas it is estimated at 1.2 eV for the Fe K-edge; the reproducibility of the monochromator is as good as 0.3 eV. The normalization procedure used throughout this work was a standard one: after subtraction of the same diffusion background on the XANES and EXAFS spectra, recorded in the same experimental conditions, a point located at an energy of 800 eV from the edge, where no more EXAFS oscillations were still observable, was set to unity. Then the intensity of a point with an energy between 50 and 100 eV from the edge was recorded on the EXAFS spectrum and reported on the XANES to set the normalization height.

Magnetism. Magnetic susceptibility $\chi(T)$ measurements were investigated in the range 5−400 K using an ac−dc SQUID Quantum Design magnetometer. For high-temperature measurements ($300 \leq T \leq 800$ K), data were collected in an applied field of 3000 G with the Faraday method using a microbalance mtb 10-8.

Results and Discussion

Structural Study. According to the synthesis method described above, a complete solid solution is obtained in the case of scandium, $Sr_4Fe_{2-x}Sc_xO_6CO_3$, $0 \leq x \leq 2$, with a color varying from dark-brown for $x = 0$ to white for $x = 2$. In the case of cobalt and nickel, the samples are black and well-sintered but the homogeneity ranges of the solid solution are more narrow: $0 \leq x \leq 1.5$ for $Sr_4Fe_{2-x}Co_xO_6CO_3$ and $0 \leq x \leq 1.1$ for $Sr_4Fe_{2-x}Ni_xO_6CO_3$. In all cases, $SrCO_3$ is always observed as an impurity (<5%) on the XRPD patterns besides the system of diffraction peaks characteristic of the $Sr_4Fe_2O_6CO_3$ structure type. In the case of nickel, small amounts of NiO are always observed as a secondary phase, whereas for the limit compound $Sr_4Sc_2O_6CO_3$ traces of $SrSc_2O_4$[9] are detected when the phase is prepared in large amounts. The EDS analyses performed on numerous microcrystals confirm the homogeneity of all the samples and show that the composition of the cobalt and scandium compounds is very close to the nominal composition, whereas in the case of nickel phases, a Ni deficiency is always observed, leading for example for $x = 1$ to the cationic composition "$Sr_4Fe_{1.1}Ni_{0.9}$".

The oxygen content determined for several samples (those studied by NPD) by redox back-titration (RBT) is found to be "6", within the limit of experimental error.

All the peaks of the XRPD patterns of these new phases can be indexed in the classical cell, $a_p \approx 3.8$, $c \approx 28$ Å, space group I4/*mmm*, characteristic of the $Sr_4Fe_2O_6CO_3$ structure, taking into consideration the presence of additional very weak peaks due to the secondary phases noted above.

The reconstruction of reciprocal space from ED patterns shows that all of the crystallites of the Ni, Co, and Sc samples exhibit a first system of intense reflections consistent with the *I*4/*mmm* space group in agreement with XRPD observations. However, in most of the crystallites, a second system of very weak reflections is present. It is similar to that observed in the case of Fe−Mn oxycarbonates and characterized by additional sharp spots at positions $^1/_2$ $^1/_2$ 0 ([001] ED patterns, Figure 2a, see white arrow) and diffuse streaky lines parallel to c^* ([$3\bar{1}0$] ED pattern, Figure 2b, see white arrow). The streaking and diffuse shape of the superlattice reflections has been interpreted as disorder phenomena in successive layers and leads us to use the space group *I*4/*mmm* for the structural calculations.

The HREM study of the Sc, Co, and Ni compounds confirms their similarity to $Sr_4Fe_2O_6CO_3$. The HREM [010] images of these compounds confirm the nature and the stacking mode of the different layers as illustrated for $Sr_4FeCoO_6CO_3$ (Figure 3), whose image is recorded to a focus value close to −15 nm, the bright dots being correlated to zones of light electronic density. The carbonate layers (see black arrows), which can easily be identified, are regularly spaced by 14 Å along $\vec{c}$.

The refined lattice parameters deduced from XRPD patterns (Table 1) show very different behavior of the Co and Ni oxycarbonates with respect to the Sc oxycarbonate. For the first ones a small and continuous decrease of *a* (0.6% for Co and 1.15% for Ni) and an increase of *c* (0.6% for both Ni and Co) are observed (Figure 4a,b) as Co or Ni is substituted for Fe, resulting in a decrease of the cell volume (Table 1) due to the smaller size of Co^{3+} and Ni^{3+} compared to that of Fe^{3+}.[10] In contrast, an expansion of the *a* value by about 4.2% and a decrease of the *c* value by about 2% is observed for the substitution of Sc for Fe (Figure 4c), leading to an increase of the cell volume with *x* (Table 1), due to the larger size of Sc^{3+} compared to that of Fe^{3+}. This different behavior of the *a* and *c* parameters of the Sc

(8) Rodriguez Carvajal, J. Collected Abstract of the Satellite Meeting on Powder Diffraction of the XVth Congr. Int. Union. Crystallographic, Toulouse, France, 1990; p 127.

(9) Carter, Feigelson, *J. Am. Ceram. Soc.* **1964**, *47*, 141.

(10) Shannon, R. D. *Acta Crystallogr.* **1976**, *A32*, 751.

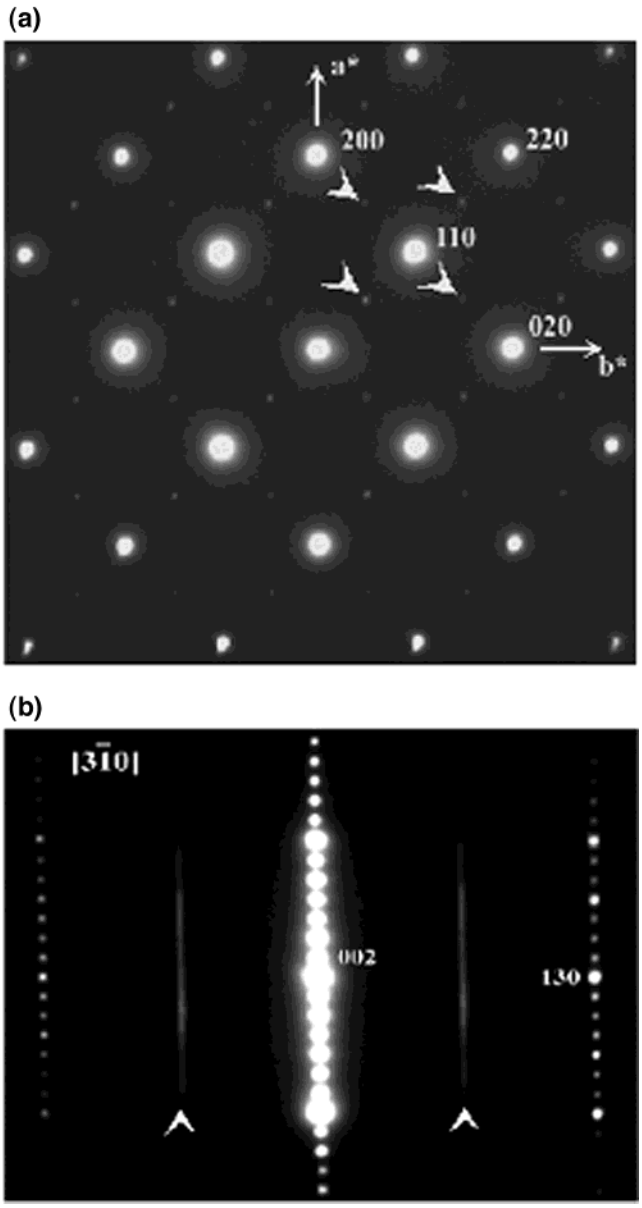

Figure 2. (a) [001] and (b) [310] ED pattern of $Sr_4FeCoO_6CO_3$.

phase with respect to Co and Ni has to be compared with the Cr phase,[6] which similarly exhibits a smaller *c* value compared to that of $Sr_4Fe_2O_6CO_3$. This suggests that the configuration of CO_3 groups is different in the Sc oxycarbonate with respect to the Co- and Ni-substituted phases. It was indeed observed that the Cr-substituted oxycarbonate is characterized by a coat hanger configuration of the CO_3 groups,[6] whereas in the pure iron phase $Sr_4Fe_2O_6CO_3$[4] a mixture of flag and coat hanger configurations is obtained.

To understand the above structural evolution, a NPD structural study has been carried out for the three following nominal compositions: $Sr_4Sc_2O_6CO_3$, $Sr_4FeCoO_6CO_3$, and $Sr_4FeNiO_6CO_3$.

For the three compounds, the calculations were carried out in the space group *I*4/*mmm* with the atomic parameters of $Sr_4Fe_2O_6CO_3$ as a starting model (i.e., a mixed flag and coat hanger configurations of the CO_3 groups). $SrCO_3$ was introduced as a secondary phase for the three compounds, whereas NiO and $SrSc_2O_4$

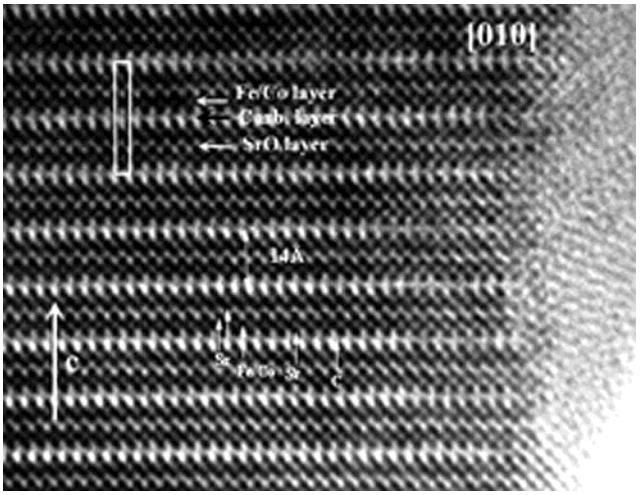

Figure 3. [010] HREM of $Sr_4FeCoO_6CO_3$.The bright dots are correlated to the light electron density zones.

Table 1. Lattice Parameters and Cell Volume for Some Oxycarbonates $Sr_4Fe_{2-x}Sc_xO_6CO_3$; Values Measured from Neutron Diffraction Patterns Are Given in Italics (Second Line)

x	*a* (Å)	*c* (Å)	*v* (Å^3)
0.0	3.8875(1)	27.979(1)	422.86(2)
	3.8888(2)	*27.982(2)*	*423.16(3)*
0.25	3.9077(3)	27.901(1)	426.05(3)
0.5	3.9288(1)	27.848(1)	429.84(2)
0.75	3.9478(2)	27.770(2)	432.79(3)
1.0	3.9672(1)	27.719(1)	436.19(2)
1.25	3.9909(1)	27.660(3)	440.54(3)
1.5	4.0102(1)	27.607(1)	443.96(2)
1.75	4.0311(2)	27.526(2)	447.29(3)
2.0	4.0529(2)	27.404(2)	450.13(4)
	4.0529(1)	*27.401(1)*	*450.12(2)*

were introduced as an impurity in the Ni and Sc compounds, respectively. In the case of scandium, the absence of structural data for $SrSc_2O_4$[9] led us to use those obtained for the isotypic phase $CaSc_2O_4$,[11] which exhibits very close lattice parameters. In the case of nickel and cobalt phases, nickel (or cobalt) and iron were statistically distributed over the same 4e crystallographic site and the occupancy factor was not refined but directly deduced from the EDS analysis, that is, FeCo (identical to the nominal one) and $Fe_{1.1}Ni_{0.9}$, respectively. For final refinements, anisotropic thermal displacements were considered except for oxygen atoms belonging to the CO_3 groups.

For the Ni and Co phases, the refinements converged to $R_p = 3.10\%$, $R_{wp} = 3.77\%$, $\chi^2 = 3.68$, and $R_B = 3.77\%$ for Ni and to $R_p = 3.78\%$, $R_{wp} = 4.75\%$, $\chi^2 = 5.08$, and $R_B = 5.05\%$ for Co. All attempts to change the carbonate groups configuration (pure flag or pure coat hanger or different ratios of those two configurations) led to unfavorable fits: $\chi^2 = 7.74$ and $R_B = 7.5\%$ for a flag configuration whether M = Ni or Co and $\chi^2 = 5.9$ and $R_B = 5.6\%$ for M = Ni and $\chi^2 = 6.70$ and $R_B = 6.2\%$ for M = Co with a coat hanger configuration. Moreover, the *U* value of the oxygen atoms involved in the CO_3 groups (O(5) and O(6) for the flag and O(3) and O(4) for the coat hanger) are much higher ($U > 0.05$ Å^2) than those obtained in the mixed flag−coat hanger configuration.

(11) Horyn, R.; Lukaszewicz, K. *Bull. Acad. Pol. Sci., Ser. Sci. Chim.* **1966**, *14*, 499 or Inorganic Crystal Structure Database file no. 16886.

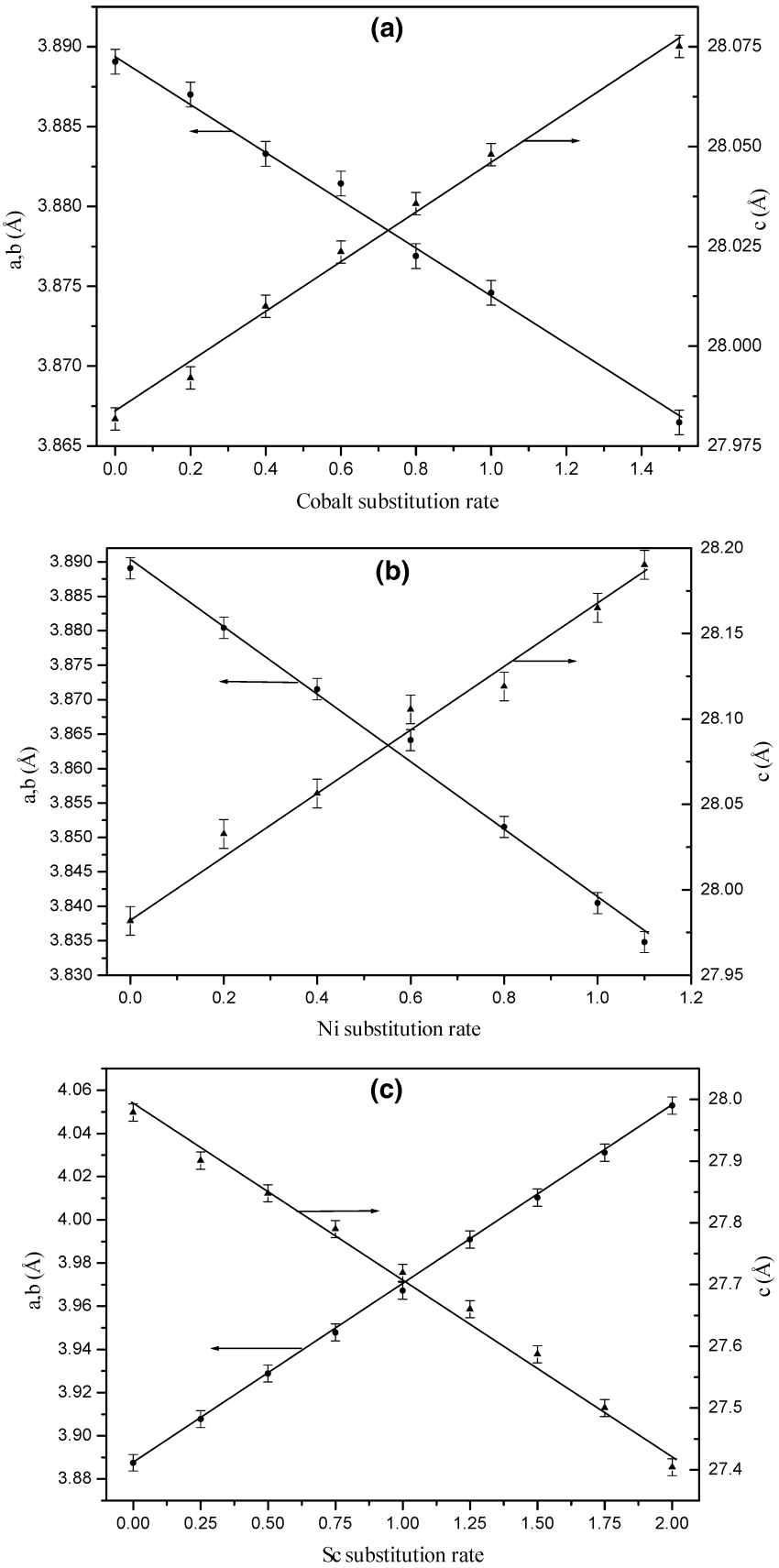

Figure 4. Evolution of the lattice constants as a function of the (a) cobalt, (b) nickel, and (c) scandium substitution rate *x*.

The final refined structural parameters are listed in Table 2 for Ni and Co, and the corresponding observed and calculated powder diffraction patterns are displayed in parts a and b of Figure 5. These results clearly establish that the positional parameters of both oxycarbonates, $Sr_4FeCoO_6CO_3$ and $Sr_4Fe_{1.1}Ni_{0.9}O_6CO_3$, are close to those obtained for $Sr_4Fe_2O_6CO_3$,[4] implying a mixture of two configurations. For the Sc phase, Sr_4-

Table 2. Structural Parameters of $Sr_4Fe_{1+x}Ni_{1-x}O_6(CO_3)$ ($x \sim 0.1$) (First Line) and $Sr_4FeCoO_6CO_3$ (Second Line, Italic Letters), Space Group *I4/mmm*

atom	site	*x*	*y*	*z*	*U* (Å²)	*n*
Sr(1)	4e	0.0	0.0	0.5728(1)		4
				0.5725(2)		
Sr(2)	4e	0.0	0.0	0.7009(1)		4
				0.7005(2)		
Fe/Ni /Co	4e	0.0	0.0	0.14284(8)		2.2/1.8
				0.1434(2)		2/2
C	2a	0.0	0.0	0.0		2
O(1)	4e	0.0	0.0	0.2107(1)		4
				0.2111(3)		
O(2)	8g	0.0	0.5	0.13147(8)		8
				0.1312(2)		
O(3)	4e	0.0	0.0	0.0515(6)	0.017(2)[a]	1
				0.0494(12)	*0.018(4)*[b]	
O(4)	16n	0.275(4)	0.0	0.0203(6)	0.017(2)[a]	2
		0.285(8)		*0.0188(12)*	*0.018(4)*[b]	
O(5)	16n	0.129(4)	0.0	0.0404(5)	0.017(2)[a]	2
		0.141(8)		*0.0386(10)*	*0.018(4)*[b]	
O(6)	8i	0.361(6)	0.0	0.0	0.017(2)[a]	1
		0.370(9)			*0.018(4)*[b]	

atom	U_{11} (Å²)	U_{22}	U_{33}	U_{eq}
Sr(1)	0.0112(8)	$=U_{11}$	0.0098(14)	0.0107(6)
	0.0093(10)		*0.0182(2)*	*0.0120(20)*
Sr(2)	0.0093(8)	$=U_{11}$	0.0089(14)	0.0092(6)
	0.0082(1)		*0.0153(2)*	*0.0080(2)*
Fe/Ni /Co	0.0049(4)	$=U_{11}$	0.0076(8)	0.0058(4)
	0.0030(10)		*0.0080(10)*	*0.0050(10)*
C	0.0189(14)	$=U_{11}$	0.0167(22)	0.0181(10)
	0.0132(20)		*0.0231(30)*	*0.0160(30)*
O(1)	0.0114(8)	$=U_{11}$	0.0024(14)	0.0084(6)
	0.0100(10)		*0.0100(20)*	*0.0100(2)*
O(2)	0.0085(10)	0.0068(10)	0.0167(14)	0.0106(4)
	0.0090(20)	*0.0120(10)*	*0.0241(20)*	*0.0150(20)*

a = 3.8405(1) Å, c = 28.165(1) Å;
$R_p = 3.10\%$, $R_{wp} = 3.77\%$, $\chi^2 = 3.68$, $R_B = 3.77\%$

a = 3.8746(1) Å, c = *28.048(1) Å;*
$R_p = 3.78\%$, $R_{wp} = 4.75\%$, $\chi^2 = 5.08$, $R_B = 5.05\%$

[a,b] Refined with the same value.

$Sc_2O_6CO_3$, with the model established for $Sr_4Fe_2O_6CO_3$ and for the Ni and Co oxycarbonates, the refinement converged to $R_p = 4.0\%$, $R_{wp} = 5.3\%$, $\chi^2 = 6.9$, and $R_B = 7.1\%$. Considering the relative high values of the agreement factors, pure flag and coat hanger configurations were tested successively. A much better fit was obtained for the pure flag configuration: $R_p = 3.3\%$, $R_{wp} = 3.9\%$, $\chi^2 = 3.9$, and $R_B = 4.8\%$. Finally, the best fit was obtained after refinement of the proportions of the two configurations, leading to 84% of the flag versus 16% of the coat hanger for the following agreement factors: $R_p = 3.2\%$, $R_{wp} = 3.8\%$, $\chi^2 = 3.7$, and $R_B = 4.4\%$. Although the improvement of the fit is not so high, it can be considered significant with regard to the 100% flag configuration since a clear decrease of the thermal displacement of the oxygens of the CO_3 groups is observed, that is, $U = 0.024$ Å² versus 0.033, 0.031, and 0.074 Å² for 100%, 50%, and 0% of the flag configuration, respectively. The observed and calculated NPD patterns (Figure 5c) attest to the goodness of the fit. The IR spectrum of this compound corroborates these results: the vibration bands in the region 500−2000 cm^{-1}, characteristic of CO_3 groups, are significantly different from those observed for $Sr_4FeCrO_6CO_3$, which exhibits exclusively in a "coat-hanger" configuration, and moreover there exists a second set of much weaker bands that can be attributed to this second configuration. The final refined atomic parameters (Table 3) are close to those observed for the other layered $Sr_4Fe_{2-x}M_xO_6CO_3$ oxycarbonates except for the CO_3 groups, which differ from both M = Fe, Co, Ni on one side and M = Cr on the other side.

Table 3. Structural Parameters of $Sr_4Sc_2O_6CO_3$

atom	site	*x*	*y*	*z*	*U* (Å²)	*n*
Sr(1)	4e	0.0	0.0	0.5705(3)		4
Sr(2)	4e	0.0	0.0	0.7016(2)		4
Sc	4e	0.0	0.0	0.1388(1)		4
C	2a	0.0	0.0	0.0		2
O(1)	4e	0.0	0.0	0.2117(3)		4
O(2)	8g	0.0	0.5	0.1271(1)		8
O(3)	4e	0.0	0.0	0.059(5)	0.024(7)[a]	0.32(7)
O(4)	16n	0.304(9)	0.0	−0.012(3)	0.024(7)[a]	0.64(7)
O(5)	16n	0.128(4)	0.0	0.0407(7)	0.024(7)[a]	3.36(7)
O(6)	8i	0.357(7)	0.0	0.0	0.024(7)[a]	1.68(7)

atom	U_{11} (Å²)	U_{22}	U_{33}	U_{eq}
Sr(1)	0.0022(6)	$=U_{11}$	0.0101(15)	0.0048(9)
Sr(2)	0.0103(7)	$=U_{11}$	0.0036(10)	0.0081(8)
Sc	0.0053(3)	$=U_{11}$	0.0126(8)	0.0077(6)
C	0.0280(14)	$=U_{11}$	0.0278(30)	0.0278(19)
O(1)	0.0322(9)	$=U_{11}$	0.0060(17)	0.0234(23)
O(2)	0.0075(6)	0.0011(5)	0.0193(11)	0.0093(14)

a = 4.0529(1) Å, c = 27.401(1) Å;
$R_p = 3.20\%$, $R_{wp} = 3.80\%$, $\chi^2 = 3.7$, $R_B = 4.45\%$

[a] Constrained to be at the same value.

Table 4. Interatomic Distances and Angles[a]

M−	O	$Fe_{1.1}Ni_{0.9}$ *d* (Å)	FeCo *d* (Å)	×*n*	Sc_2 *d* (Å)	×*n*
Sr(1)−	O(2)	2.533(2)	2.541(6)	×4	2.552(5)	×4
	O(3)	2.781(4)	2.815(9)	×1	2.89(2)	×0.32
	O(4)	2.57(1)	2.59(2)	×1	2.70(5)	×0.32
	O(5)	2.56(1)	2.57(2)	×1	2.65(1)	×1.68
	O(6)	2.860(5)	2.853(9)	×1	2.859(8)	×1.68
Sr(2)−	O(1)	2.488(4)	2.479(9)	×1	2.376(9)	×1
	O(1)	2.730(1)	2.756(1)	×4	2.879(1)	×4
	O(2)	2.741(3)	2.746(5)	×4	2.876(4)	×4
Fe/M−	O(1)	1.912(4)	1.90(1)	×1	1.998(9)	×1
	O(2)	1.947(1)	1.968(2)	×4	2.052(6)	×4
	O(3)	2.57(2)	2.64(3)	×0.25	2.24(9)	×0.08
	O(5)	2.93(1)	2.99(3)	×0.5	2.74(2)	×0.84
C−	O(3)	1.45(2)	1.38(3)	×0.5	1.56(9)	×0.16
	O(4)	1.20(2)	1.22(3)	×1	1.27(4)	×0.32
	O(5)	1.24(2)	1.21(2)	×1	1.23(2)	×1.68
	O(6)	1.39(2)	1.43(4)	×0.5	1.45(3)	×0.84
		O(4)−O(3)−O(4) Triangle				
O(3)−C−O(4)		118.4(8)	115.5(7)		105(3)	×2
O(4)−C−O(4)		123.0(10)	129.0(10)		150(5)	×1
		O(5)−O(6)−O(5) Triangle				
O(5)−C−O(5)		132.8(10)	126.6(10)		130(1)	×1
O(5)−C−O(6)		113.6(7)	116.7(8)		115.0(8)	×2

[a] In the distance list, the numbers of the neighboring oxygen atoms of the elements (*n*) are calculated by taking into account the oxygen site occupancies.

The interatomic distances (Table 4) show that in the three compounds the coordination of cobalt, nickel, and scandium is very similar and can be described as a tetragonal pyramid. Four equatorial M−O bonds of 1.95−1.97 Å for cobalt (or nickel) and 2.05 Å for scandium are observed, whereas the apical M−O bond is much shorter, that is, 1.90−1.91 Å for Co (Ni) and 1.99 Å for Sc. In all cases a sixth oxygen neighbor sits much farther apart, at 2.55−2.99 Å for Co and Ni and at 2.24−2.74 Å for scandium. The CO_3 groups are characterized by two short C−O bonds and a long one

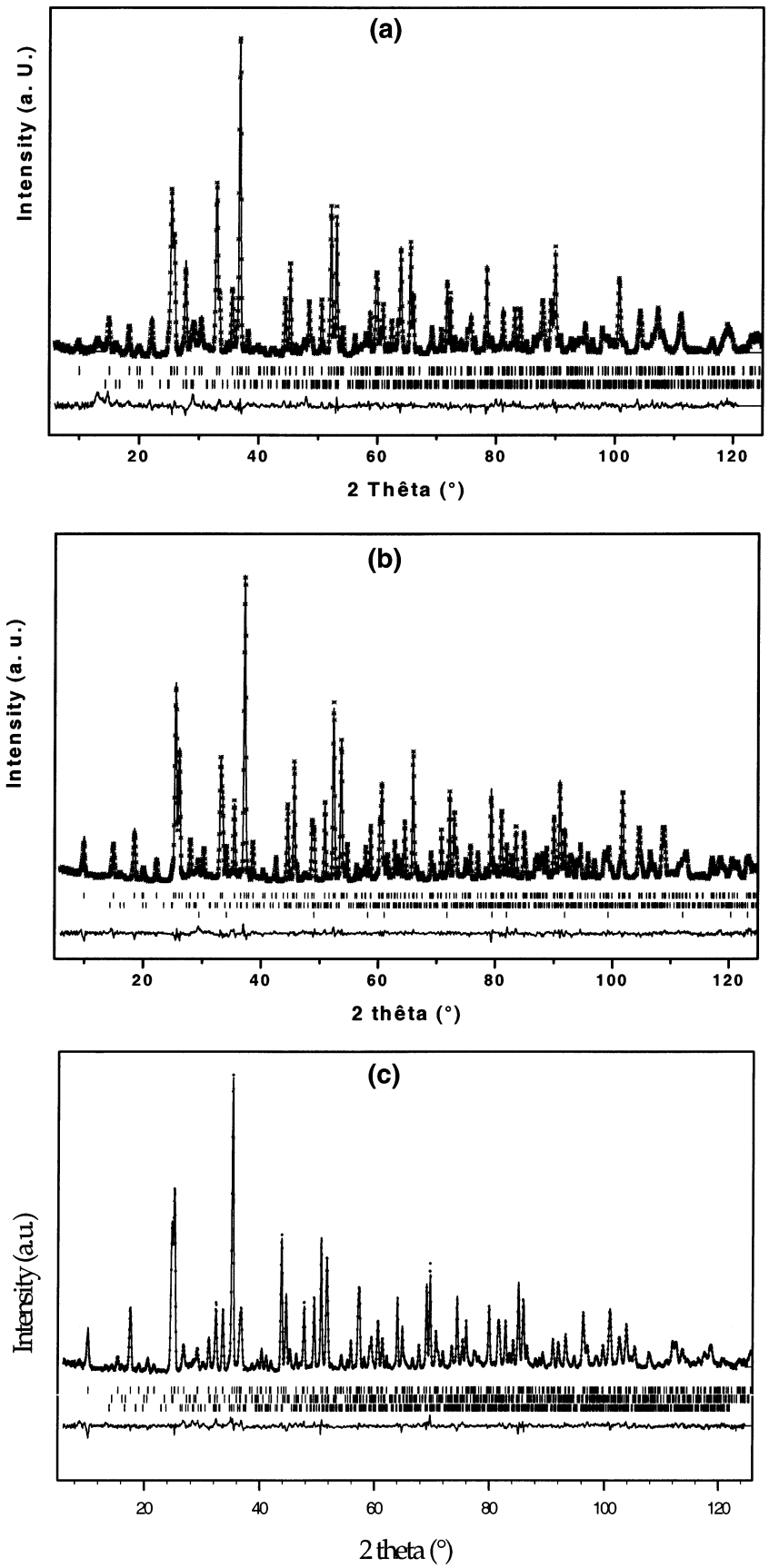

Figure 5. Experimental (crosses), calculated, and difference (solid lines) neutron powder diffraction patterns of (a) Sr_4FeCoO_6-CO_3, (b) $Sr_4Fe_{1.1}Ni_{0.9}O_6CO_3$, and (c) $Sr_4Sc_2O_6CO_3$ at the end of refinement. The vertical bars are the Bragg angle positions for the main phase (upper) and the impurity $SrCO_3$ (lower for Co and middle for Ni) and NiO (lower) and $SrSc_2O_4$ (lower).

whatever their configuration, coat hanger (compare for instance the C−O(3) and C−O(4) distances in the three compounds) or flag (compare the C−O(5) and C−O(6) distances). The O−C−O angles range from 113° to 132°

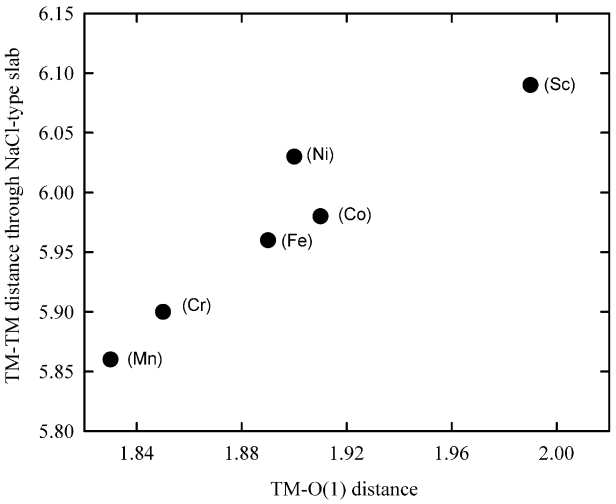

Figure 6. Apical TM−O(1) distance (d3) versus TM−TM distance through a NaCl-type slab (d2).

Table 5. Lattice Parameters, $(Fe_{1-x}M_x)-(Fe_{1-x}M_x)$ Distances along *c* through CO_3 Groups (d_1) and a NaCl-Type Slice (d_2) and $(Fe_{1-x}M_x)-O(1)$ (d_3) Distances in the Oxycarbonates $Sr_4Fe_{1-x}M_xO_6CO_3$ from Room Temperature Neutron Diffraction Data

composition	*a* (Å)	*c* (Å)	d_1 (Å)	d_2 (Å)	d_3 (Å)
$Sr_4Sc_2O_6CO_3$	4.0529(1)	27.401(1)	7.60(4)	6.09(4)	1.998(9)
$Sr_4FeCrO_6CO_3$	3.8948(8)	27.696(8)	7.94(7)	5.90(7)	1.854(8)
$Sr_4FeMnO_6CO_3$	3.8569(2)	28.272(2)	8.27(7)	5.86(7)	1.828(6)
$Sr_4Fe_2O_6CO_3$	3.8888(1)	27.982(1)	8.03(4)	5.96(4)	1.889(9)
$Sr_4FeCoO_6CO_3$	3.8746(1)	28.048(1)	8.04(7)	5.98(7)	1.90(1)
$Sr_4Fe_{1.1}Ni_{0.9}O_6CO_3$	3.8405(1)	28.165(1)	8.05(3)	6.03(3)	1.912(4)

whatever the configuration. Note that the C−O distances and O−C−O angles for the coat hanger configuration of the Sc oxycarbonate cannot be considered as accurate due to the small content of this configuration, contrary to $Sr_4FeCrO_6CO_3$[6] for which the latter is the unique one. In the Cr oxycarbonate the triangular groups are, in contrast to the other ones, particularly regular with C−O bonds ranging from 1.24 to 1.25 Å and O−C−O angles ranging from 114° to 123°. The FeO_5 pyramid is more compressed than in the other oxycarbonates with four identical equatorial bonds (1.97 Å) and one very short apical bond, that is, 1.85 Å. The CrO_6 octahedra are distorted with four equatorial bonds (1.97 Å) and an abnormally very short apical bond (1.85 Å) opposed to a long one (2.46 Å).

The distance between two successive $(Fe_{1-x}M_x)$ transition metals (TM), which sandwich a carbonate layer, varies significantly with the ionic radii nature (d1 in Table 5) of the transition metal. It is higher for the oxycarbonates that contain mixed configurations of the CO_3 groups ($Sr_4Fe_2O_6CO_3$, $Sr_4FeCoO_6CO_3$, $Sr_4Fe_{1.1}Ni_{0.9}O_6CO_3$, and $Sr_4FeMnO_6CO_3$) than for compounds that contain mainly one kind of CO_3 group ($Sr_4FeCrO_6CO_3$ and $Sr_4Sc_2O_6CO_3$); it increases with increasing *c*. This suggests that disorder at the level of the CO_3 configurations tends to induce an increase of the TM−TM distances and consequently to increase the *c* parameters. Through the NaCl-type slice the TM−TM distance (d2) seems directly correlated to the apical TM−O(1) distance (d3), as shown in Figure 6. This implies that the thickness of the rock-salt-type slice remains almost constant (2.10−2.20 Å) whatever the nature of TM.

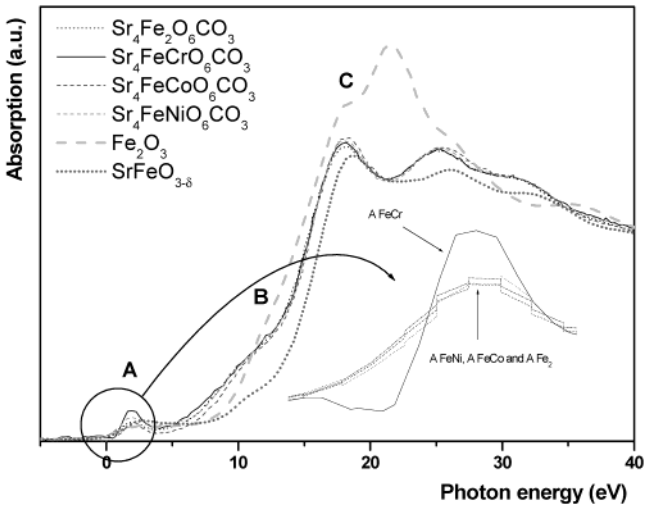

Figure 7. XANES normalized Fe K-edges at room temperature for iron references and for $Sr_4FeCoO_6CO_3$ and $Sr_4Fe_{1.1}Ni_{0.9}O_6CO_3$.

XANES Study of the Ni and Co Oxycarbonates. In contrast to scandium, for which the oxidation state Sc^{3+} is the only possibility, nickel and cobalt offer various oxidation states that cannot be foreseen due to the possible redox equilibrium $Fe^{3+} + M^{3+} \leftrightarrow M^{2+} + Fe^{4+}$. To determine the oxidation state of nickel and cobalt in these compounds, a XANES study has been performed at Fe, Co, and Ni K-edges on five oxycarbonates $Sr_4Fe_{2-x}M_xO_6CO_3$, that is, $x = 0.5$ and 1 for M = Ni and $x = 0.1$, 1, and 1.5 for Co.

Iron K-Edge. The Fe K-edge spectra of the two compounds $Sr_4FeCoO_6CO_3$ and $Sr_4FeNiO_6CO_3$, compared to the reference compounds $Sr_4Fe_2O_6CO_3$ (Fe^{3+}) and $Sr_4FeCrO_6CO_3$ (Fe^{3+}) and $SrFeO_{3-\delta}$ (Fe^{4+}) are shown on Figure 7. The energy at midheight of the main absorption jump (Table 6) allows the iron oxidation state to be estimated at +3 for the Co and Ni oxycarbonates. Note that in the two cases there is no evolution of the latter whatever the value of *x*.

One can see that spectra of the two Fe/Co and Fe/Ni samples are unchanged and identical to that of $Sr_4Fe_2O_6CO_3$, contrary to that of $Sr_4FeCrO_6CO_3$ for which the prepeak labeled A_{Cr} is more intense. This suggests that, in the mixed Co/Fe or Ni/Fe oxycarbonates, the iron environment should be the same as that in the $Sr_4Fe_2O_6CO_3$ oxycarbonate and different from that in the mixed Cr/Fe oxycarbonate in which the sixth oxygen (O_3) is sitting too far away, leading to a true pyramidal environment for iron.

Cobalt and Nickel K-Edge. The Co K-edge of the three mixed Fe/Co oxycarbonates under consideration and of two reference oxides $LaCoO_3$ (for Co^{3+}) and $CoCO_3$ (for Co^{2+}) are shown in Figure 8. Note that the three spectra are identical and the energy at midheight of the main absorption jump allow the cobalt oxidation state to be fixed to +3. The relative intensities of the prepeaks A due to a strong hybridization of Co(3d)−O(2p)−Co(4p) orbitals indicate a non-centrosymmetric environment like pyramidal, which is compatible with the structural results. In the same way the Ni K-edge of the two mixed Fe/Ni compounds and of two reference oxides $LaNiO_3$ (for Ni^{3+}) and $NiCO_3$ (for Ni^{2+}) are shown in Figure 9. The two spectra are identical and the energy at mid-

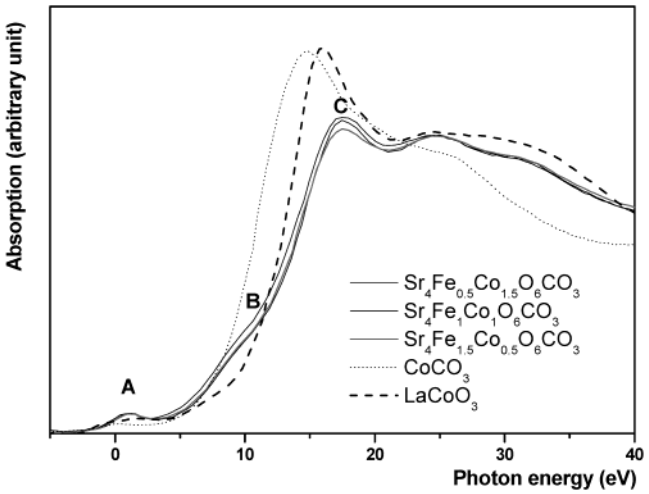

Figure 8. XANES normalized Co K-edges at room temperature for cobalt references and for nominal compositions of $Sr_4Fe_{2-x}Co_xO_6CO_3$, $x = 0$, 0.5, 1, and 1.5.

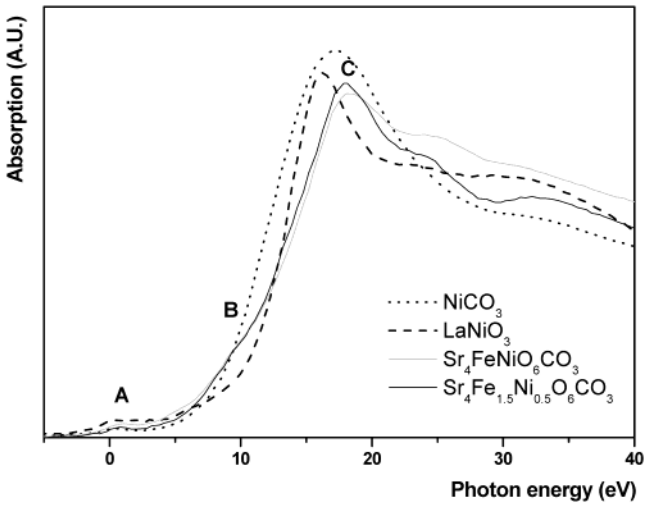

Figure 9. XANES normalized Ni K-edges at room temperature for nickel references and for nominal compositions of $Sr_4Fe_{2-x}Ni_xO_6CO_3$, $x = 0.5$, and 1.

height of the main absorption jump allow the nickel oxidation state to be fixed to +3. The prepeaks A indicate a non-centrosymmetric environment compatible with the neutron results.

Whatever M and x (0.5, 1, 1.5), one can see the similarity between the Fe and Co or Ni K-edge spectra. This is in agreement with the neutron diffraction results for which the iron and nickel or cobalt atoms are distributed over the same crystallographic site, implying the same environment. The peaks labeled B could be correlated to the 1s−4p transition corresponding to nonbonding orbitals pointing toward long M−O distances, whereas the peaks labeled C are correlated to the 1s−4p transition corresponding to bonding orbitals pointing toward the short M−O distances.

Within the limit of the technique accuracy we can admit that there is no evolution of the oxidation state of the species Fe, Co, and Ni in the series $Sr_4Fe_{2-x}M_xO_6CO_3$.

Magnetic Properties. As expected, the pure scandium phase does not exhibit any magnetism. In contrast, the Co and Ni phases are of interest.

In the case of the Ni oxycarbonate, the presence of NiO as an impurity requires some attention for the study of the magnetic properties of $Sr_4Fe_{1.1}Ni_{0.9}O_6CO_3$. Using NiO as a reference, we have measured for both compounds, NiO and the oxycarbonate, the magnetic susceptibility using ac and dc methods and we have checked that the magnetic contribution of NiO was much smaller than that of the oxycarbonate and could be neglected, taking into account the estimated NiO amount (2.3 wt %) deduced from neutron diffraction data. For $T \geq 300$ K the linear part of $\chi^{-1}(T)$ (inset Figure 10) of $Sr_4Fe_{1.1}Ni_{0.9}O_6CO_3$, fitted with a Curie−Weiss law $\chi = \chi_0 + c/T - \theta P$, where C is the Curie constant, θ_P the paramagnetic Curie temperature, and χ_0 the temperature-independent susceptibility, leads to an effective magnetic moment of 7.35 μ_B/mol, which is close to the expected one calculated by considering Fe^{3+} and Ni^{3+} in a high-spin configuration ($\mu_{eff} = 7.21\ \mu_B$). The low θ_P value (−714.5 K), deduced from this extrapolation, is characteristic of strong antiferromagnetic fluctuations in the paramagnetic regime for this compound. It has been predicted by Goodenough[12] that the

Table 6. Formal Charge (F.C.), d_{M-O}, Energy of Main Jump Midheight (E.M.J.M.) at Fe K-edge, Co K-edge, and Ni K-Edge for References and Compounds under Consideration

compounds	F.C.	d_{M-O} (Å)	E.M.J.M. (eV) ± 0.3 eV
Fe_2O_3	+3	1.94 × 3	13.6
		2.11 × 3	
$Sr_4Fe_2O_6CO_3$	+3	1.97 × 4	13.9
		1.90 × 1	
		2.60 × 0.25	
		2.94 × 0.5	
$Sr_4FeCrO_6CO_3$	+3	1.97 × 4	13.9
		1.85 × 1	
$Sr_4FeCoO_6CO_3$	+3	1.97 × 4	13.9
		1.90 × 1	
		2.64 × 0.25	
		2.99 × 0.5	
$Sr_4Fe_{1.1}Ni_{0.9}O_6CO_3$	+3	1.95 × 4	13.9
		1.91 × 1	
		2.57 × 0.25	
		2.93 × 0.5	
$SrFeO_3$	+4	1.92 × 4	15.2
		1.98 × 2	
$CoCO_3$	+2	2.15 × 3	10.7
$Sr_4Fe_{1.5}Co_{0.5}O_6CO_3$	+3	1.97 × 4	12.8
		1.90 × 1	
		2.64 × 0.25	
		2.99 × 0.5	
$Sr_4FeCoO_6CO_3$	+3	1.97 × 4	12.8
		1.90 × 1	
		2.64 × 0.25	
		2.99 × 0.5	
$Sr_4Fe_{0.5}Co_{1.5}O_6CO_3$	+3	1.97 × 4	12.9
		1.90 × 1	
		2.64 × 0.25	
		2.99 × 0.5	
$LaCoO_3$	+3	1.95 × 6	12.8
$NiCO_3$	+2	2.07 × 6	10.5
$Sr_4Fe_{1.5}Ni_{0.5}O_6CO_3$	+3	1.95 × 4	12.1
		1.91 × 1	
		2.57 × 0.25	
		2.93 × 0.5	
$Sr_4Fe_{1.1}Ni_{0.9}O_6CO_3$	+3	1.95 × 4	12.2
		1.91 × 1	
		2.57 × 0.25	
		2.93 × 0.5	
$LaNiO_3$	+3	1.96 × 6	12.2

(12) Goodenough, J. *Magnetism and the Chemical Bond*; Interscience: New York, 1963.

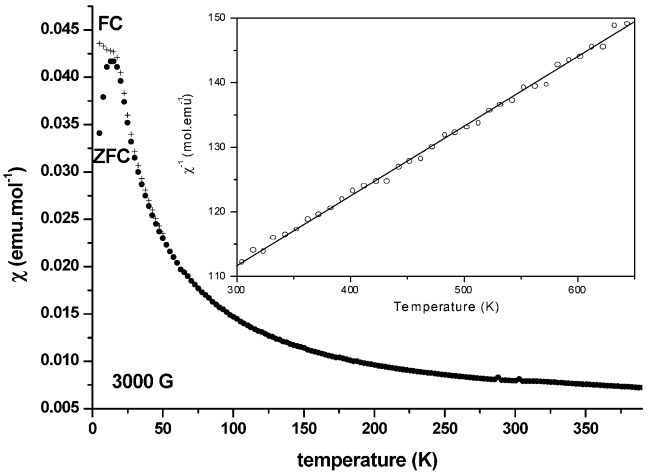

Figure 10. $\chi_M(T)$ curves of $Sr_4Fe_{1.1}Ni_{0.9}O_6CO_3$ obtained from the ZFC and FC $M(T)$ curves recorded in 3000 G. $\chi^{-1}{}_M(T)$ curve (open circles are experimental points whereas the solid line is the fit).

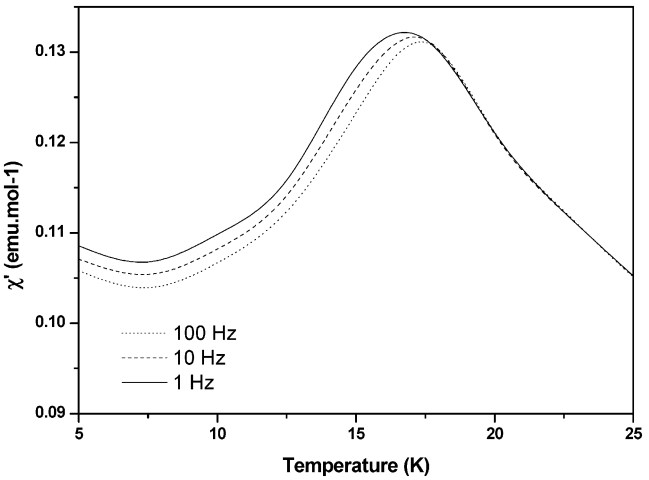

Figure 11. Real part (χ') of the ac−χ versus T for $Sr_4Fe_{1.1}Ni_{0.9}O_6CO_3$. The frequencies are labeled in the graph.

superexchange between Ni^{3+}(HS) and Fe^{3+}(HS) ions is antiferromagnetic, which is also the case for the cations of same spins (Fe^{3+}/Fe^{3+}, Ni^{3+}/Ni^{3+}). One would thus expect an antiferromagnetic transition for this composition. Furthermore, the strong 2D nature of $Sr_4Fe_{1.1}Ni_{0.9}O_6CO_3$ implies the existence of magnetic anisotropy: in the perovskite block, the AFM coupling is expected to be stronger than the magnetic coupling between blocks. Consequently, since the in-plane magnetic 2D correlations first develop and then the out-of-plane magnetic ordering at a lower temperature, complex magnetic behaviors are also expected. The magnetic susceptibility measurements performed in the range 5−400 K in an applied field of 3000 G (ZFC−FC method) are shown in Figure 11. In contrast to the FC curve, which exhibits increasing values as T decreases from 300 K down to the lowest temperatures with a slowing down below about 17 K, starting from 5 K the ZFC M values first increase as T increases to reach a maximum at ∼17 K and then decrease beyond that temperature. The ZFC and FC curves merge just at the temperature of the χ maximum on the ZFC part. This shape of the curve, showing a clear magnetic transition, suggests a spin glass behavior at low temperature. To check that point, ac−χ data have been collected using a SQUID

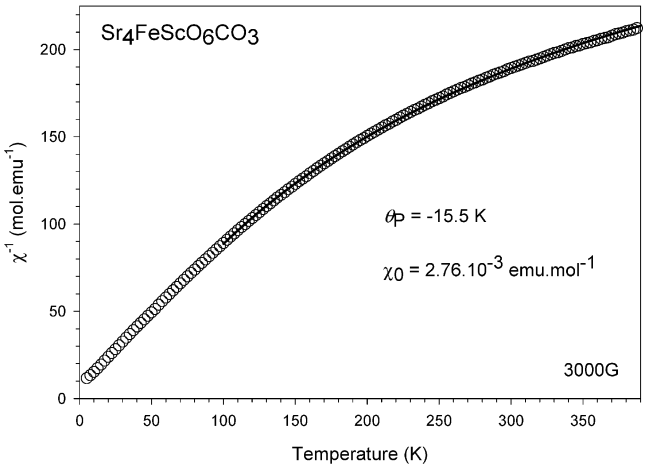

Figure 12. $\chi^{-1}{}_M(T)$ curves of $Sr_4FeScO_6CO_3$ obtained from the ZFC $M(T)$ curve recorded in 3000 G (open circles are experimental points whereas the solid line is the fit).

magnetometer, with hac = 3 Oe, without a dc magnetic field ($h_{dc} \sim 0$) and with three frequencies: 1, 10, and 100 Hz. The real part χ' (T) curve (Figure 11) shows a cusplike shape peaking at about 17.5 K, and below this temperature, the curves registered for the different frequencies start to separate with the largest χ' value observed for the smallest f as expected for a spin glass. Clearly, as the frequency increases, T_f, defined as the χ' maximum value on the $\chi'(T)$ curve, increases from 16.8 to 17.4 K for 1 and 100 Hz respectively, leading to a K value of 0.018 (with $K = \Delta T_f/T_f\Delta(\log \omega)$ where ω is the frequency), which is a typical value for spin glasses. According to the weak magnetism generally observed for nickelates containing trivalent Ni^{3+} such as in $LaNiO_3$,[13] the large Ni^{3+} content substituted for Fe^{3+} creates a severe dilution of the $Fe^{3+}-O-Fe^{3+}$ antiferromagnetic array. This situation is similar to the situation encountered in the $Rb_2Cu_{1-x}Co_xF_4$[14] layered compound where the antiferromagnetic Co interactions are diluted by the Cu cations, leading to spin glass behavior for $0.18 \leq x \leq 0.40$. In that case, the bond randomness was invoked to explain the origin of the spin glass state,[14] which is also the case for $Sr_4Fe_{1.1}Ni_{0.9}O_6CO_3$.

In contrast, the $\chi(T)$ data of $Sr_4FeCoO_6CO_3$, collected in the range 5−800 K in a magnetic field of 3000 G, exhibit quasi T independent χ values with χ in the range 0.39−0.41 emu mol^{-1}. This indicates that the paramagnetic T region is not reached even at $T \approx 800$ K. It suggests that the ordering temperature of this phase is higher than 800 K or that a ferromagnetic impurity with $T_C > 800$ K is responsible for the observed behavior. Note that, despite all our attempts, no impurity phase has been revealed by the electron microscopy observations.

The $\chi(T)$ curve of $Sr_4FeScO_6CO_3$, collected in the range 5−400 K, shows paramagnetic-like behavior for the whole T range. However the $\chi^{-1}(T)$ curve is better fitted in the range 100−400 K with the Curie−Weiss law: $\chi = \chi_0 + c/T - \theta P$ (Figure 12). From the θ_P value (−15.5 K), it can be concluded that some antiferromag-

(13) Garcia-Munoz, J. L.; Rodriguez Carvajal, J.; Lacorre, P.; Torrance, J. B. *Phys. Rev. B, Condens. Matter. Mater. Phys.* **1992**, *16*, 4414.

(14) Mydosh, J. A. *Spin glasses: an experimental introduction*; Taylor and Francis: London, 1993.

netic $Fe^{3+}-O-Fe^{3+}$ fluctuations persist. This suggests that Fe^{3+} clusters exist in this compound that are responsible for the very weak antiferromagnetism revealed by the magnetic data. Nevertheless, no clear magnetic transition can be detected, in agreement with the electron microscopy observations, which evidenced a random distribution of iron and scandium. The Curie–Weiss fit leads also to an effective paramagnetic moment μ_{eff} of 5.6 μ_B, which agrees with the expected value for high spin (HS) Fe^{3+} (5.9 μ_B).

The present magnetic study, revealing very distinct magnetic behaviors for the three isostructural compounds ($Sr_4FeScO_6CO_3$, $Sr_4FeCoO_6CO_3$, and $Sr_4Fe_{1.1}Ni_{0.9}O_6CO_3$) under study, deserve a study of the magnetic structure by neutron powder diffraction.

Acknowledgment. The authors are indebted to Dr. Françoise Bourée and Mr. Bernard Rieu (Laboratoire Léon Brillouin, Saclay, France) for collection of neutron diffraction data, and to Dr. M. Daturi (Laboratoire de Catalyse et Spectrochimie, Caen, France).

CM020468W